



Removal of malachite green from water: Comparison of adsorption in a residue-derived AC versus photocatalytic oxidation with TiO₂ and study of the adsorption-photocatalysis synergy

S. Boumad^{a,b}, L. Cano-Casanova^a, M.C. Román-Martínez^a, N. Bouchenafa-Saib^b, M.A. Lillo-Ródenas^{a,*}

^a MCMA Group, Department of Inorganic Chemistry and Materials Institute (IUMA), University of Alicante, Ap. 99, E-03080 Alicante, Spain

^b Université Blida 1, Laboratoire de Chimie Physique des Interfaces des Matériaux Appliquées à l'Environnement, Faculté de Technologie, B.P. 270 Route de Soumaa, 09000 Blida, Algeria

ARTICLE INFO

Keywords:

Malachite green
Water treatment
Luffa activated carbon
Simulated solar light
Adsorption
Photooxidation with TiO₂

ABSTRACT

The literature rarely compiles studies devoted to the removal of pollutants in aqueous media comparing adsorption and photocatalytic degradation, and does not pay enough attention to the analysis of combined adsorption-photocatalytic oxidation processes. In the present manuscript, the removal of malachite green (MG) from aqueous solutions has been investigated in three different sustainable scenarios: i) adsorption on activated carbon (AC) derived from a residue, luffa cylindrica, ii) photocatalytic oxidation under simulated solar light using titanium dioxide (TP) and iii) combined adsorption-photocatalytic oxidation using TP-AC (70/30 wt./wt.) under simulated solar light. The study has revealed that in the three scenarios and studied conditions, the total removal of this endocrine-disrupting dye from the solution takes place in the assayed time, 2 h, in some cases just in a few minutes. MG adsorption in the AC is a very fast and efficient removal method. MG photocatalytic oxidation with TP also occurs efficiently, although the oxidized MG is not totally mineralized. MG removal using the TP-AC composite under simulated solar light occurs only slightly faster to the MG adsorption in the AC, being adsorption the dominating MG removal mechanism for TP-AC. Thus, more than 90% of the removed MG with TP-AC under simulated solar light is adsorbed in this carbon-containing composite. The obtained results highlight the interest in adsorption, being the selection of the most suitable removal method dependent on several factors (i.e., the cost of the AC regeneration, for adsorption, or the toxicity of the intermediate oxidation species, for photooxidation).

Paying attention to MG photooxidation with TiO₂, comparison of two working photodegradation schemes shows that the direct photodegradation of MG from solution, avoiding any initial dark equilibrium period, is more efficient from a time perspective. The use of scavengers has proved that MG photodegradation occurs via an oxidation mechanism dominated by superoxide anion radicals.

1. Introduction

Malachite green (MG) is a well-known synthetic dye used in the textile industry, in the paper dyeing process, and as a food coloring agent (Ahmad and Kumar, 2010; Srivastava et al., 2004; El-Zahhar and Awwad, 2016). It is a triphenylmethane cationic dye, environmentally recalcitrant, and extremely toxic to a variety of aquatic and terrestrial mammals, being carcinogenic and a multi-organ toxin for humans (Bello et al., 2015), and considered an endocrine-disrupting dye. Despite being

banned in several countries, it is still extensively used in the aquaculture industry, i.e., as a fungicide and for protozoan infections in fish (Cooksey, 2016). Thus, the removal of dyes, such as malachite green, from wastewater is an important challenge for society, and the subject of several studies over the last few years (Lin et al., 2016; Das et al., 2009; Farooqi et al., 2020).

Among the different alternatives for the removal of undesirable organic and inorganic impurities from domestic and industrial wastewater, adsorption is one of the most used methods (Xu and Liu, 2008). It

* Corresponding author. Department of Inorganic Chemistry. University of Alicante, San Vicente del Raspeig (Alicante). PO BOX 99. E-03080, Spain.
E-mail address: mlillo@ua.es (M.A. Lillo-Ródenas).

is effective and fast, its design is simple, its operating cost is low and it avoids the production of harmful by-products (Bhatnagar and Anastopoulos, 2017). For this purpose, different materials, such as carbonaceous materials, biomass, clays, zeolites, etc., can be used as adsorbents (Al Bahri et al., 2012; Cruz et al., 2018). Among them, activated carbons (AC) have been extensively used as versatile adsorbents due to their well-developed porous structure and tunable properties (Bansal and Goyal, 2005). Despite these outstanding properties, once the adsorbent is saturated, an additional regeneration step is needed for further use (Hernández, 2012). To overcome this, and to enhance the pollutants removal, attempts for the combination of adsorption and advanced photocatalytic oxidation processes have been carried out (Wang et al., 2018).

Heterogeneous photocatalysis is considered one of the most promising processes for wastewater treatment, given its potential for complete mineralization of pollutants to non-toxic products. It implies using a semiconductor that is excited by UV or visible light, being the created electron/hole pairs responsible for the redox reactions that lead to the pollutants degradation (Regalbuto, 2006; Zhang et al., 2014; Guimarães et al., 2012; Kisch, 2015). Many semiconductors, such as ZnO, CuO, Ga₂O₃, have succeeded to be suitable as photocatalysts, and titanium dioxide (TiO₂) is among the preferred ones because of its high chemical stability and low cost, being environmentally friendly. Heterogeneous photocatalysis is not only suitable for the oxidation of organic compounds, but also for the inactivation of microorganisms (Bansal et al., 2009; Gao et al., 2015; Reddy et al., 2015). However, it also has some drawbacks, such as the high rate of electron/hole (e⁻/h⁺) pairs recombination, and the hard sedimentation and difficult separation in liquid processes, given its small particle size (Araña et al., 2003). Improving the TiO₂ efficiency is, for all these reasons, indeed interesting.

If an adsorbent and a photocatalyst are combined, the pollutant becomes concentrated close to the photocatalytic active sites, which can enhance its removal (Liu et al., 2007; Paušová et al., 2019). For that purpose, zeolites and silica have been widely studied as TiO₂ “additives” (Devi and Kavitha, 2014; Lucas et al., 2013), but AC has especially gained many researchers’ attention because of its well-known adsorption capacity (Andriantsiferana et al., 2014; Nitnithiphrut et al., 2017; Slimen et al., 2011). The synergistic photodegradation of organic pollutants when AC is combined with TiO₂ has been reported, and it is explained as a result of the formation of a contact interface between both solid phases and the transfer of the pollutants adsorbed on activated carbon to titania, where they are directly photodegraded (Araña et al., 2003; Matos et al., 2001). Furthermore, TiO₂ particles could be well dispersed on the activated carbon surface, avoiding their agglomeration (Che Ramli et al., 2014; Morawski et al., 2009). Additionally, in some conditions, carbon atoms can be incorporated into the titania network, creating new energy levels just above the valence band of TiO₂ and reducing the bandgap, which could also explain a photodegradation activity enhancement in some particular cases (Lavand et al., 2019).

Among the experimental parameters of the photocatalytic process, the irradiation source is of great importance. Different light sources (i.e. solar light irradiation, or artificial sources, such as UV lamps or simulated solar light) have been employed for the photocatalytic degradation of malachite green using TiO₂ (Bojinova et al., 2007; Arifin et al., 2015). As an example, Ju et al. have studied the microwave-assisted photocatalytic degradation of malachite green in aqueous TiO₂ suspensions using UV irradiation of electrodeless discharge lamps (EDLs) (Ju et al., 2008). Bojinova et al. have reported the photocatalytic degradation of malachite green under UV irradiation using titanium dioxide photocatalysts with different anatase/rutile ratios (Bojinova et al., 2007). The photodegradation of malachite green under UV and visible light at different pH values has also been examined by Sayilkan et al. using Sn-doped TiO₂ (Sayilkan et al., 2007). Yong et al. have studied the photodegradation rates and pathways of malachite green under natural and simulated irradiation without the addition of catalysts, finding that

suitable conditions of pH (between 5 and 9) and concentration (10 mg/L) accelerate the degradation process of this dye in natural waters (Yong et al., 2015).

The literature survey highlights the lack of studies that perform a systematic comparison between adsorption and photocatalytic degradation of pollutants, such as MG, in aqueous media. Also, to the best of our knowledge, no published studies focus on the photocatalytic degradation of the malachite green dye using titania-activated carbon hybrids under simulated solar light. Therefore, in the present study, the removal of MG from solution under simulated solar light using a titania/activated carbon hybrid material is investigated, and compared with the MG removal by adsorption in the same activated carbon, that has been obtained from *Luffa cylindrica* (see section A and Fig. S1 in the Supplementary Material), and by photocatalytic degradation using a TiO₂ photocatalyst. Thus, on one hand, this study contributes to the proper selection of the most suitable method for the removal of MG and related compounds from solution, either by adsorption or by solar light-driven photocatalytic degradation, not usually compared in similar experimental conditions. On the other hand, it deepens into the role of incorporating carbon, leading to titania-activated carbon composites, analyzing the MG removal rate, and trying to determine which of the two processes, adsorption or photodegradation, controls the MG removal, and which are the possible intermediation degradation products, if any. Finally, it enlightens the mechanism governing the photocatalytic oxidation of MG with TiO₂, performing tests with different scavengers.

2. Experimental section

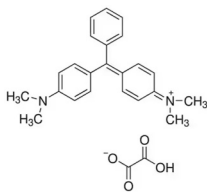
2.1. Materials and reagents

Commercial P25 (Aeroxide) titanium dioxide was provided by Degussa. Phosphoric acid (H₃PO₄, 85 wt % solution) was purchased from Panreac. 1,4-benzoquinone (C₆H₄O₂, 108.09 M, 99%), methanol (99.8%), 2-propanol (C₃H₈O, ≥99.5%) and malachite green oxalate (N, N', N'-Tetramethyl-4,4'-diamino-triphenyl-carbenium oxalate (see Table 1)) were purchased from Sigma-Aldrich. All the reactants have been used without further purification.

2.2. Activated carbon preparation

Activated carbon was prepared by chemical activation with H₃PO₄ of *Luffa cylindrica* fibers collected in Algeria (see additional information in the Supplementary Material, section A and Fig. S1). The vegetal fibers were rinsed several times with distilled water to remove dust and organic impurities, and dried in an oven at 90 °C overnight. The dried

Table 1
Physicochemical properties of the malachite green dye (information extracted from the product specification sheet from the official site of Sigma Aldrich).

Property	Property Value
Molecular Weight	463.50 g mol ⁻¹
Empirical formula	C ₂₃ H ₂₅ N ₂ · C ₂ HO ₄ · 0.5C ₂ H ₂ O ₄
Structure	 <chem>CN(C)C1=CC=C(C=C1)C(=O)C(=O)N(C)C</chem> • 1/2 C ₂ H ₂ O ₄
Appearance (Form)	Solid crystals
Color	Faint green to very dark green
Solubility	1 mg mL ⁻¹ , H ₂ O.
Color	Blue to very dark blue
Dye Content	>99.5 %
PKa	6.9

fibers were cut into small pieces and, after milling and sieving, the fraction of size $>800 \mu\text{m}$ was collected. The activation procedure, previously reported (Bouchenafa-Saïb et al., 2005), is as follows: the pre-treated Luffa fibers and an 85 wt.% phosphoric acid solution (H_3PO_4 /luffa fibers ratio of 3/1 wt./wt.), were mixed and kept in contact for 3 h. The resulting mixture was heated at $5^\circ\text{C}/\text{min}$ up to 500°C in a tubular furnace and maintained at that temperature for 1 h before letting to cool down. After cooling, the obtained solid was washed several times with distilled water to a neutral pH, removing chemicals after the activation process. The prepared activated carbon was named AC.

2.3. TiO_2 and TiO_2 -based materials

Commercial TiO_2 (P25) supplied by Degussa (named TP) was used without further modification/purification. The hybrid photocatalyst containing AC and TiO_2 was prepared by mechanical mixing in an agate mortar (MM), using 0.3 g AC and 0.7 g TP. This TiO_2 /AC proportion was selected according to previous publications (Bouazza et al., 2008; Lillo-Ródenas et al., 2007). The obtained sample was denoted as TP-AC.

2.4. Characterization of the prepared materials

The morphology of the three prepared samples was investigated using a scanning electron spectroscopy instrument (Quattro S model, FEI) at 10 kV and 3.0 spot.

The evaluation of the textural properties of the materials was conducted by N_2 adsorption-desorption at -196°C and CO_2 adsorption at 0°C in a Quantachrome Autosorb-6B apparatus. The samples were previously degassed at 250°C for 4 h. The specific surface area (S_{BET}) and the total micropore volume ($V_{\text{DR}} \text{N}_2$) were determined using, respectively, the Brunauer-Emmett-Teller equation and the Dubinin-Radushkevich equation, applied to the N_2 adsorption data (Rodríguez-Reinoso and Linares-Solano, 1988; Cazorla-Amorós et al., 1996). The mesopore volume (V_{meso}) was estimated by the difference of the volume of N_2 adsorbed at $P/P_0 = 0.9$ and $P/P_0 = 0.2$, expressed as a liquid (Romero-Anaya et al., 2012). The total pore volume (V_{T}) was determined from the volume of nitrogen adsorbed at a $P/P_0 = 0.99$.

Attention has also been paid to the surface properties of AC and TP. The pHs of zero charge of the surface (pHpzc) of the different samples were determined by potentiometric titration according to the protocol of Kummert and Stumm (1980). The titration was performed using nitric acid, HNO_3 (0.01M), or sodium hydroxide, NaOH (0.01M), added to a solution of 0.1g of sample in 100 mL of distilled water. The surface charge was determined using the following equation:

$$q = \frac{(C_a - C_b - [\text{H}_3\text{O}^+] + [\text{OH}^-])}{m} \quad (1)$$

where:

- q: the surface charge ($\text{mol}\cdot\text{g}^{-1}$);
- C_a : the concentration of acid after addition ($\text{mol}\cdot\text{L}^{-1}$);
- C_b : the concentration of base after addition ($\text{mol}\cdot\text{L}^{-1}$);
- $[\text{H}_3\text{O}^+]$ and $[\text{OH}^-]$: the concentrations of these ions, according to the measured pH (both in $\text{mol}\cdot\text{L}^{-1}$);
- m: the sample mass in ($\text{g}\cdot\text{L}^{-1}$).

The crystallinity of the samples was determined by X-ray diffraction (XRD). XRD patterns were recorded for the samples mixed with CaF_2 (50/50, wt./wt.) using the equipment Miniflex II Rigaku (30 kV/15 mA) with $\text{Cu K}\alpha$ radiation at a scanning velocity of $2^\circ/\text{min}$, in the 2θ range $6-80^\circ$. The Scherrer equation (Equation (2)) was used to calculate the average crystallite size as follows:

$$B = \frac{K\lambda}{\beta \cos \theta} \quad (2)$$

where B is the average crystallite size (nm); K is the Scherrer constant ($K = 0.93$), λ is the radiation wavelength (0.1540 nm for $\text{Cu K}\alpha$), β is the full width at half maximum intensity (FWHM) and θ is the Bragg angle associated to the main peak of the studied phase (2θ values of 25.3 and 27.5° for anatase and rutile, respectively). The percentage of anatase (A %), rutile (R%), and amorphous phase were calculated as reported in ref. (Amorós-Pérez et al., 2018), see equations (3) and (4):

$$A(\%) = \frac{\frac{A_{\text{anatase}(101)}}{A_{\text{CaF}_2(220)}} \times 100}{1.25} \quad (3)$$

$$R(\%) = \frac{\frac{A_{\text{rutile}(110)}}{A_{\text{CaF}_2(220)}} \times 100}{0.9} \quad (4)$$

where $A_{\text{anatase}(101)}$, $A_{\text{rutile}(110)}$, and $A_{\text{CaF}_2(220)}$ are the peak areas extracted from XRD spectra measured for a 50/50 (wt./wt.) mixture of TiO_2 / CaF_2 . The constants 1.25 and 0.9 are the theoretical ratios between areas of the same peaks when a 100% anatase or 100% rutile crystalline titania sample is used.

UV-vis/Difuse Reflectance spectroscopy (JASCO V-670 spectrometer) equipped with an integrating sphere accessory was used to investigate the optical absorption properties of the samples. The reflectance signal was calibrated by a Spectralon standard (Labsphere SRS-99-010, 99%), using BaSO_4 as the reference standard. The band gap energy (E_g) was calculated by two different methods, the absorbance method, and the indirect allowed transition. In the absorbance method, the band gap energy values, in eV, were calculated as:

$$E_g = \frac{1239.8}{\lambda} \quad (5)$$

where λ is the absorption edge wavelength, in nm, obtained from the intersection of a fitted tangent to the absorbance UV curve with the wavelength axis at which the absorbance is equal to zero.

In the indirect method, this form of the Tauc equation was used:

$$(\alpha h\nu)^{1/2} = B(h\nu - E_g) \quad (6)$$

where α is the absorption coefficient, h is the Planck constant, ν is the frequency and B is a constant. The plot of $(\alpha h\nu)^{1/2}$ vs $h\nu$ allows to obtain E_g .

2.5. Malachite green removal

The removal of MG from aqueous solution (10 mg L^{-1}) by adsorption or photocatalytic degradation was studied in the present study.

Two adsorption equilibrium tests with AC and the MG aqueous solution (10 mg L^{-1}) were performed to determine the adsorption capacity at room temperature (25°C) and with the vessel reactor introduced in an ice bath ($5-25^\circ\text{C}$). In these tests, 20 mg of the AC were in contact for 2 h with 500 mL of 10 mg L^{-1} of MG aqueous solution. The purpose of these tests was to determine the equilibrium adsorption capacity of the AC at the two assayed temperatures.

In the MG adsorption kinetics or photocatalytic degradation tests, the following general conditions were used: 250 mL of a malachite green solution with an initial MG concentration of 10 mg L^{-1} and 0.125 g of photocatalyst or adsorbent (TP-AC, TP or AC) were continuously stirred in a Pyrex glass vessel. The suspension was sonicated for 2 min to achieve good dispersion.

For the photodegradation experiments, the vessel was introduced in an ATLAS SUNTEST CPS + instrument with a xenon arc lamp for simulated natural solar radiation (See Fig. S2a in the Supplementary Material, section B). Two photodegradation schemes were assayed: a) the solution was maintained in the dark for 1 h before irradiation, to establish adsorption-desorption equilibrium, or b) MG solution irradiation occurred from the beginning of the test.

It must be pointed out that the temperature of the solution increases

upon irradiation in the ATLAS SUNTEST chamber. In particular, in the photodegradation scheme based on dark for 1 h followed by irradiation, the photocatalytic process occurs in the temperature interval from 25 °C to 45 °C (see Fig. S2b in the Supplementary Material, section B). To avoid such temperature increase, experiments were carried out also with the vessel reactor introduced in an ice bath. In this case, the temperature of the reaction media varied from 5 °C to 25 °C (see Fig. S2c in the Supplementary Material, section B). These two temperature conditions are denoted MT and LT, meaning moderate and low temperature, respectively, and are being commented on in this study.

For the adsorption kinetic experiments, with AC, TP and TP-AC, the reaction vessel was left all the time in the dark, and two temperature regimes were assayed, at room temperature (25 °C) and with the vessel reactor introduced in an ice bath (5-25 °C).

Both during the MG photodegradation and the adsorption tests, 4 mL of solution were taken from the vessel at fixed time intervals, filtered, and analyzed by UV-vis spectrophotometry (Shimadzu PC1201) to determine the MG concentration (by means of the maximum absorbance, at 618 nm). The concentration of malachite green in each test was assessed using a linear-fit calibration plot.

The correct interpretation of the experiments has required performing additional tests to understand and evaluate the results from the MG removal experiments. In particular, in section C in the Supplementary Material, blank tests (using AC but in the absence of any photocatalyst) evaluating the MG removal from the solution that could occur by combining a dark period followed by simulated solar light, or by the direct irradiation scheme are included (see Section C and Fig. S3 in the Supplementary Material). Also, section D in the Supplementary Material shows a photolysis test (without photocatalyst) over the MG solution, carried out to evaluate the potential photochemical degradation of MG (Fig. S4 in the Supplementary Material).

The total organic content (TOC) of the MG initial solution ($t = 0$ min), as well as the TOC values of the solutions (for MT conditions), were measured after 60, 120, and 180 min of irradiation using the TP photocatalyst and a TOC-VCSH/CSN Shimadzu equipment.

To evaluate which MG intermediate oxidation species could appear, the analysis of the solutions after 60, 120, and 180 min of irradiation using the TP photocatalyst, as well as the analysis of the MG initial solution ($t = 0$ min), was performed using gas chromatography coupled to mass spectrometry (GC-MS) in a 5975C Agilent equipment. The column used was an Agilent 19091s-433hp-5ms (30 m \times 250 μ m \times 0.25 μ m). The protocol used included a first stage at 40 °C for 5 min, followed by a heating step at 12 °C \cdot min $^{-1}$ up to 290 °C, held for 6 min, and, finally at 20 °C \cdot min $^{-1}$ up to 320 °C, held for 10 min.

To unveil the mechanism of the MG photocatalytic degradation, a study with different interfering agents (scavengers) was conducted with TiO₂ TP. Methanol, benzoquinone, and 2-propanol were used as inhibitors of photogenerated positive holes (h^+), superoxide anion radicals ($O_2^{\bullet-}$), and hydroxyl radicals (HO^{\bullet}), respectively. In each case 2 mL of the scavenger solution (0.2 mol/L) were added to the MG solution.

3. Results and discussion

3.1. Characterization of the prepared samples

3.1.1. Morphology characterization by scanning electron microscopy

Section E and Fig. S5 in the Supplementary Material compile some information for the AC, TP and TP-AC samples obtained by SEM, including images obtained with the same magnification. The typical porous morphology of an activated carbon, resulting from the activation with phosphoric acid, is shown in Figs. S5a and S5b (in the Supplementary Material). Figs. S5c and S5d from the Supplementary Material contain the SEM micrographs for TP sample, confirming the porosity in the TiO₂ (P25) sample. Regarding the TP-AC sample, with 70/30 TiO₂/AC (weight ratio), it can be noticed that TP is well dispersed on the AC surface, covering homogeneously most of its surface (Figs. S5e and S5f

from the Supplementary Material). No significant agglomeration of TP particles on the AC surface is observed.

3.1.2. Crystallinity characterization by X-ray diffraction

XRD analysis has been performed to evaluate the crystallinity of the different samples. The corresponding patterns are presented in Fig. 1. The characteristic XRD peaks of the TiO₂ phases were observed. The 2θ values for anatase and rutile (Cano-Casanova et al., 2018; Nitnithiphрут et al., 2017; Fu et al., 2004) (in brackets the corresponding families of planes) are the following.

- **Anatase:** 25.3° (101); 37.8° (004); 48.0° (200); 54.5° (105); 55.0° (211); 62.7° (204); 70.4° (116); 74.5° (220)
- **Rutile:** 27.5° (110); 36.1° (101); 41.1° (111); 54.4° (211); 76.5° (202)

For the AC, a broad diffraction feature located at $2\theta \sim 24^\circ$ is found, showing that it is not crystalline. XRD profiles for TP and TP-AC are very similar and reveal that they mainly contain anatase with some rutile.

Analysis of the XRD spectra show that the proportion of amorphous TiO₂ in the samples is about 14%, and the anatase and rutile contents are about 73% and 13%, respectively. The crystallite size of these two phases is 21 and 29 nm, respectively. These data are, in agreement with data reported in the literature (Sing et al., 2014; Ohtani et al., 2010) and in a previous study (Cano-Casanova et al., 2018).

3.1.3. Textural characterization by physical adsorption of gases

N₂ adsorption-desorption isotherms of samples TP, TP-AC, and AC are compiled in Fig. 2. They are all type IV according to the IUPAC classification, corresponding to mesoporous materials (Thommes et al., 2015). An important microporous contribution is observed for the isotherms of AC and TP-AC, which indeed can be identified as a combination of type I+IV isotherms. The adsorption capacity of each sample is quite different, and also the samples show a different type of hysteresis

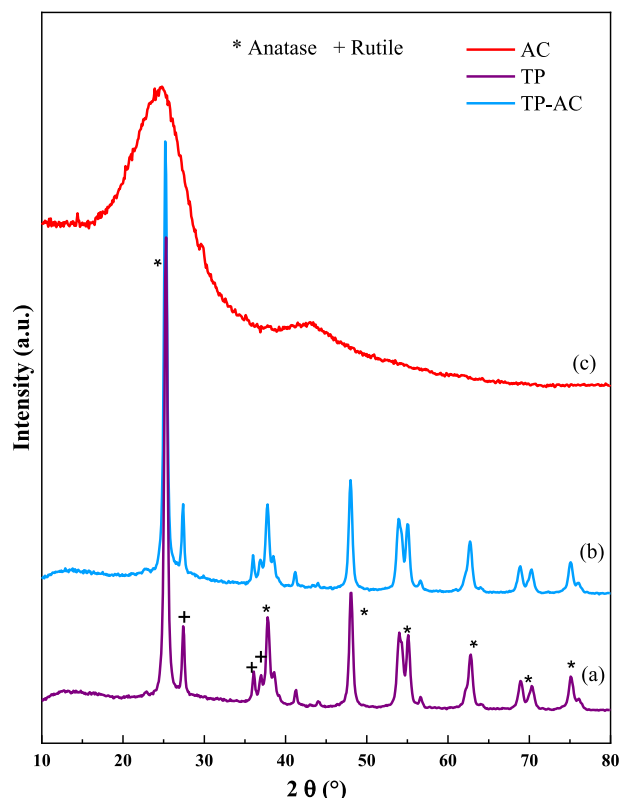


Fig. 1. XRD patterns for (a) TP, (b) TP-AC, and (c) AC.

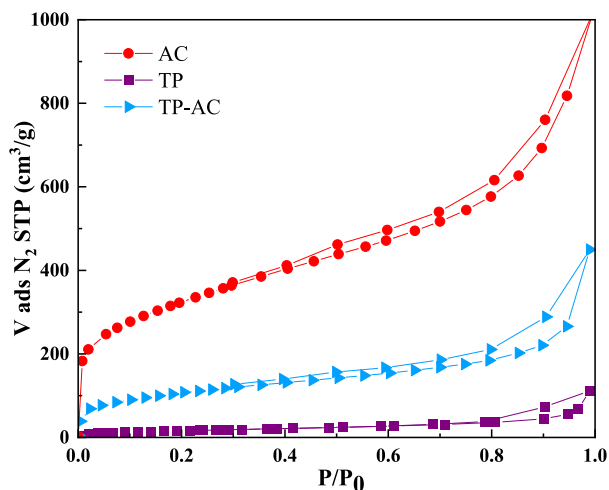


Fig. 2. N_2 adsorption-desorption isotherms at $-196\text{ }^\circ\text{C}$ for the prepared materials: AC, TP and TP-AC.

loop, H3 for sample TP and H4 for samples AC and TP-AC, indicating some differences in the mesoporosity structure of TP and AC (Thommes et al., 2015).

Table 2 summarizes the textural properties for the studied materials, determined from the adsorption data. The Luffa-derived AC shows a high surface area, and the S_{BET} determined for TP, much lower, is in agreement with the values reported in the literature (Cano-Casanova et al., 2018; Liu et al., 2007). The surface area of the TP-AC composite is the expected one according to the proportion of TP (70 wt.%) and AC (30 wt.%) present in it.

3.1.4. Surface chemistry and point of zero charge characterization

The surface chemistry of AC, TP and TP-AC samples has been previously investigated using Fourier transform infrared (FTIR) analysis (Cano-Casanova et al., 2021; Boumad et al., 2021). The obtained spectra showed the presence of a medium height peak at around 3700 cm^{-1} , associated to O–H bond, and the absorption band of water molecules appeared at 1680 cm^{-1} . Two bands in the range $2200\text{--}2300\text{ cm}^{-1}$ are associated to CO_2 vibration band and medium $\text{C}=\text{C}$ stretching band. A strong absorption peak, attributed to the Ti–O–Ti bond, was observed around $850\text{--}1200\text{ cm}^{-1}$.

The surface properties of the AC-containing samples have been characterized paying attention to the oxygen-containing functional groups, as they strongly influence their quality as adsorbents.

The points of zero charge (see Fig. 3) were found to occur approximately at pH values of 6.6, 6.5, and 6.7 for TP, AC, and, TP-AC, respectively. These pH_{pzc} values for AC, TP and TP-AC indicate some dominance of acidic functional groups on the surface (Kosmulski, 2021). The pH_{pzc} values imply that the surface is positively charged in the solution up to these pH values, and negatively charged above these pHs (László, 2005). Taking into account the composition of TP-AC, an expected pH_{pzc} for TP-AC would be 6.6. Being MG a cationic dye, its adsorption is supposed to be favored when the pH of the medium is higher than the pH_{pzc}.

Table 2

Textural parameters of the synthesized samples, obtained from N_2 adsorption-desorption at $-196\text{ }^\circ\text{C}$ and CO_2 adsorption at $0\text{ }^\circ\text{C}$.

	$S_{\text{BET}} [\text{m}^2\text{g}^{-1}]$	$V_{\text{Total}} [\text{cm}^3\text{g}^{-1}]$	$V_{\text{DR}} (N_2) [\text{cm}^3\text{g}^{-1}]$	$V_{\text{MESO}} [\text{cm}^3\text{g}^{-1}]$	$V_{\text{DR}} (\text{CO}_2) [\text{cm}^3\text{g}^{-1}]$
AC	1139	1.15	0.48	0.66	0.19
TP	60	0.10	0.02	0.08	0.02
TP-AC	383	0.34	0.16	0.28	0.07

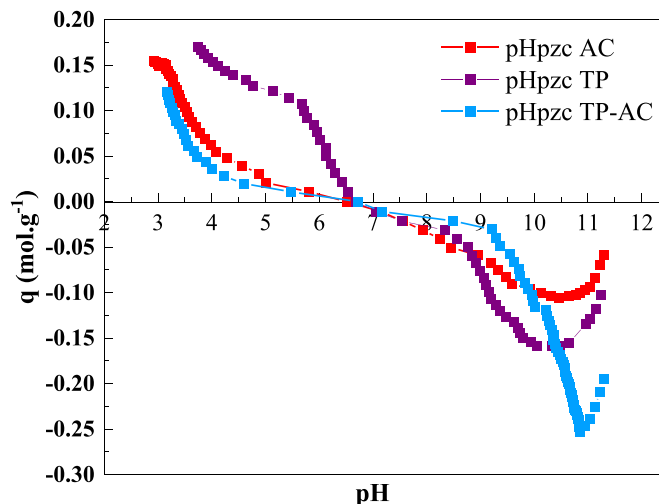


Fig. 3. Surface charge versus pH curves for AC, TP, and TP-AC samples.

3.1.5. Optical properties determined by UV–vis analysis

The UV–vis diffuse reflection spectra of the samples are included in the Supplementary Material (Fig. S6 in section F in the Supplementary Material). According to the spectra, in the UV region, the lowest absorption occurs for TP, whereas the absorption for TP-AC is slightly enhanced in this region, as a result of the highest absorption registered for AC.

Table 3 presents the E_g values calculated by both, the absorbance and the indirect transition methods, showing that they are in good agreement. The E_g value for TP-AC is lower than that for TP, which can be attributed to the presence of AC. Note the high absorbance of the activated carbon in a large range of wavelengths, especially in the visible region, in agreement with previously published data (Shahcheragh et al., 2023).

3.2. Malachite green removal

3.2.1. Adsorption equilibrium tests

The adsorption equilibrium tests on AC at low and moderate temperatures have shown that, for the 10 mg L^{-1} MG aqueous solution, the AC equilibrium adsorption capacities are 160 and 150 mg MG/g of AC, respectively.

Considering that the adsorption kinetic tests are being performed using 250 mL of MG solution with 10 mg L^{-1} concentration and 0.125 g of photocatalyst or adsorbent, in the adsorption kinetic tests the ratio amount of MG to be removed/amount of adsorbent is well below the MG adsorption capacity of the AC.

Table 3

Energy band gap (E_g) values obtained from absorbance method, and the indirect allowed transition one for TP and TP-AC.

Sample	E_g (eV) ^a	E_g (eV) ^b
TP	3.05	3.07
TP-AC	2.46	2.47

^a absorbance.

^b indirect method.

3.2.2. Adsorption kinetic tests (in darkness)

Fig. 4 plots the MG adsorption data determined in dark conditions at the two temperatures. Comparing both temperature ranges, the difference in the adsorption capacity is negligible. The adsorption of MG in TP is, as expected, negligible. An important MG adsorption capacity is noted in AC, attributed to its high surface area of $1139 \text{ m}^2/\text{g}$ and developed porous texture. Although the $\text{pH}_{\text{pzc}} > \text{pH}$, AC has a very high MG adsorption capacity. Note that the amount of MG to be adsorbed in these tests is one order of magnitude lower than the MG adsorption capacity for the AC in these conditions.

The removal of MG by adsorption in TP-AC is also similar to that in AC.

3.2.3. Tests under simulated solar light: photocatalytic degradation/adsorption processes

As explained, two schemes have been assayed: a) before irradiation, the solution was maintained in the dark for 1 h to establish adsorption-desorption equilibrium, which was then followed by irradiation of the MG solution, or b) the irradiation of the MG solution occurred from the beginning of the test. The tests were repeated twice to check reproducibility, and the experimental errors were below 7 %.

The removal of the MG dye for TP, TP-AC, and AC samples under solar light, expressed by the variation of C/C_0 versus time in the two steps experiments, is compiled in Fig. 5. Note that the correct interpretation of Fig. 5 requires to consider the blank experiments (included in Fig. S3 in the Supplementary Material), and the photolysis data (Fig. S4 in the Supplementary Material). The photolysis tests, that is, the study of MG degradation in the absence of photocatalyst, showed that photochemical degradation of MG does not occur, being MG photochemically stable under the studied conditions.

Fig. 5 confirms that, as expected, TP showed a low MG adsorption in dark, lower than 10% of the MG initial concentration, whereas the composite TP-AC, as well as the AC, showed a high (and similar) MG adsorption, ranging 90–95% of the initial MG concentration. This behavior is attributed to the porosity of the activated carbon (see Table 2), and agrees with the data presented in Fig. 4.

Once the solution was exposed to irradiation, the photodegradation of MG from the solution over TP occurred within the time assayed. In fact, total removal of MG from the solution is achieved with the three materials. In AC and TP-AC, most of the MG removal occurs in the dark period and is a consequence of MG adsorption, whereas more than 90% removal of MG was achieved with TP via photooxidation within 60 min of irradiation. The temperature had very little effect on the MG removal performance, being the results for the two studied temperature ranges very similar.

Data in Fig. 5 and Fig. S3 (in the Supplementary Material) indicate that MG removal in TP-AC composite is slightly enhanced (comparing to the AC) due to the presence of TP.

A second set of experiments was conducted starting with the irradiation of simulated solar light once the materials and MG solution were put in contact (Fig. 6). The correct interpretation of data in Fig. 6, which shows a very similar performance for both temperature regimes, implies taking into consideration the adsorption results, compiled in Fig. 4, and the blank and photolysis tests (Figs. S3 and S4 in the Supplementary Material).

Data of Fig. 6 shows that the removal of MG from solution is achieved with the three materials, TP, AC and TP-AC, within the time assayed. The results for the two studied temperature ranges are similar, as clearly observed in Fig. S7 and section G from the Supplementary Material.

A slightly faster MG removal kinetics is observed in the TP-AC sample, consequence of the combination of adsorption and photo-degradation processes occurring simultaneously in this material. In fact, some literature studies suggest that the photocatalytic process is boosted by the adsorption of the organic compound on the AC of the composite, promoting the transfer of the organic compound molecules to the surface of the photocatalytic active sites.

Not only the removed MG, but also the percentage of remaining TOC are of interest to evaluate the degree of mineralization of the malachite green. In the experiment using TP as photocatalyst (Fig. 6), the TOC values have been measured at $t = 0$ (initial MG solution) and after 60, 120 and 180 min of irradiation. The percentages of removal of TOC after 60, 120 and 180 min of irradiation using the TP photocatalyst are 51, 70 and 75 %. This implies that although most MG is oxidized in short time, it is not totally mineralized, and some MG intermediate oxidation species exist.

GC-MS analysis of the solutions after 60, 120 and 180 min of irradiation using the TP photocatalyst has been performed aiming to determine if any MG intermediate oxidation compounds could be detected, confirming the presence of 4-(methylamino)benzophenone, [4-(1-cyclohexyl)-(1'-phenyl)-methyl]-2,4-hexenoic acid, benzaldehyde and hydroquinone, in agreement with previous publications (Pérez-Estrada et al., 2008; Fischer et al., 2011; Song et al., 2020).

To analyze what is occurring in the removal of MG by the TP-AC composite, and by the rest of materials studied, a tentative analysis of such removal has been performed at a certain time (10 min, see Table 4), considering the MG removal by adsorption (from data in Fig. 4) and the MG removal under illumination (from data in Fig. 6). The percentage of MG removal by photodegradation has been estimated as the corresponding subtraction.

Data of Figs. 4 and 6 and Table 4 highlight that adsorption governs

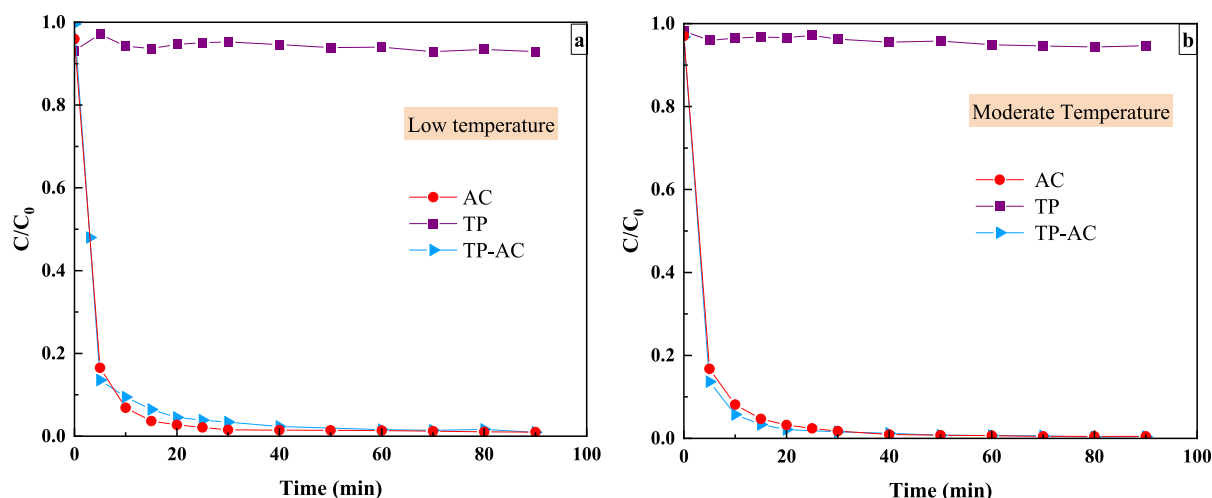


Fig. 4. MG adsorption in dark conditions at low (a) and moderate temperature (b) using: $m_{\text{solid}} = 0.125 \text{ g}$, $V_{\text{solution}} = 250 \text{ mL}$, $C_0 \text{ (MG)} = 10 \text{ mg/L}$, $\text{pH} = 5.8$.

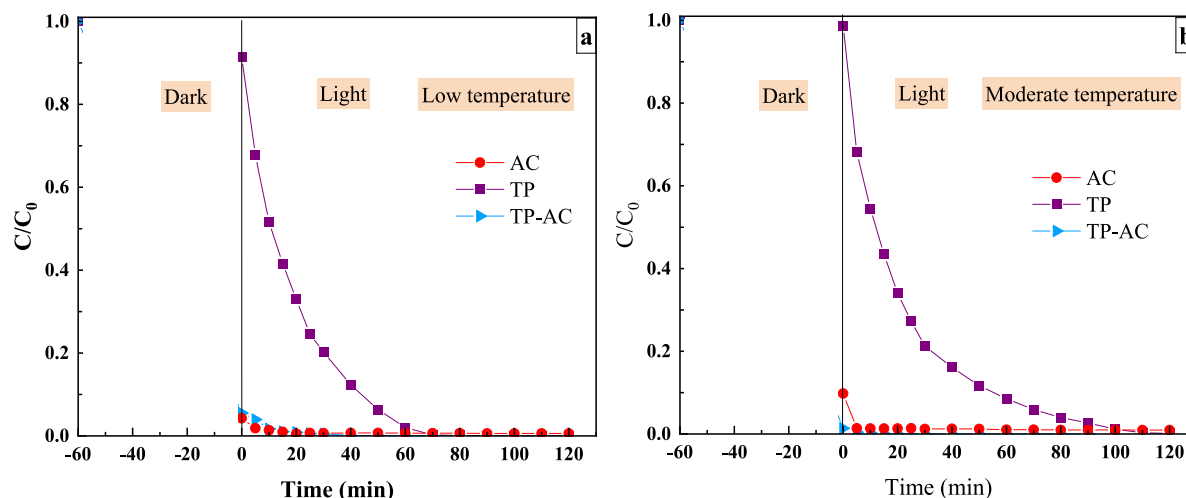


Fig. 5. Removal of MG using TP, TP-AC and AC under dark followed by simulated solar light irradiation at low (a) and moderate (b) temperature in the following conditions: $m_{\text{solid}} = 0.125$ g, $V_{\text{solution}} = 250$ mL, C_0 (MG) = 10 mg/L, pH = 5.8.

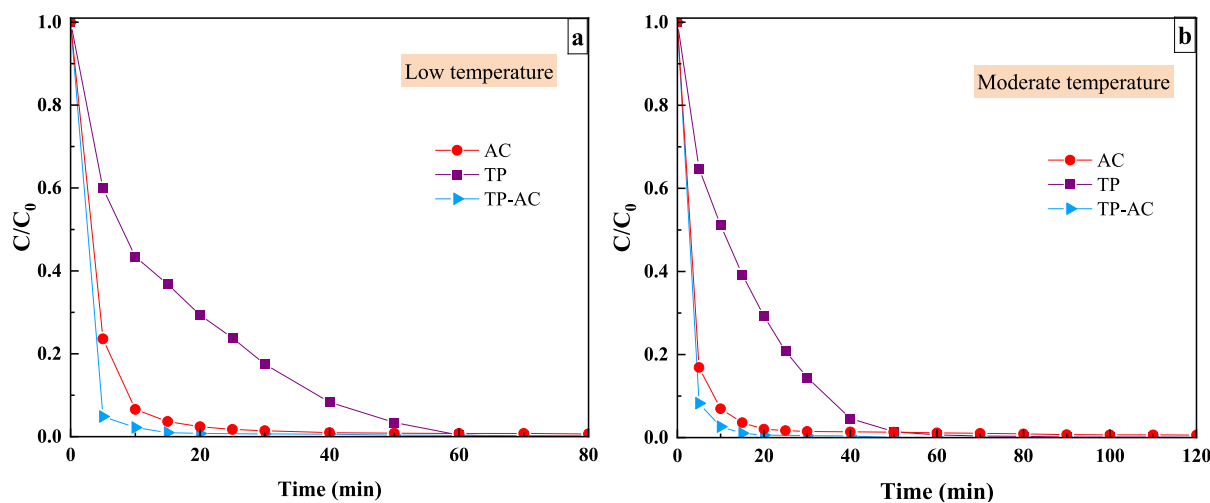


Fig. 6. Removal of MG under simulated solar light in presence of TP, TP-AC and AC: (a) at low temperature and (b) at moderate temperature. Conditions: $m_{\text{solid}} = 0.125$ g, $V_{\text{solution}} = 250$ mL, C_0 (MG) = 10 mg/L, pH = 5.8.

Table 4

Quantitative analysis of the MG removal by adsorption and photodegradation from the kinetic tests (at 10 min time).

		Samples		
		AC	TP	TP-AC
Removed MG ^a	Q1: % MG removed by adsorption (From data in Fig. 4)	92	3	92
	Q2: % MG removed under illumination (From data in Fig. 6)	92	53	97
	Q2-Q1: % MG removed by photodegradation	0	50	5

^a At $t = 10$ min; Q: quantity of MG removed, expressed in (%).

MG removal in AC and TP-AC, although some photooxidation of MG also occurs in TP-AC due to the presence of TP. Note that TP-AC contains 70 wt.% of TP.

Further analysis needs to be done to evaluate the relative importance of adsorption and photocatalytic degradation in MG removal by TP-AC, as it will be done next paying attention to the photodegradation mechanism.

From the comparison of Figs. 5 and 6, it can be concluded that, as could be expected, performing the direct removal of MG dye without

reaching the adsorption equilibrium is faster for TP-AC and, especially for TP, which is important for saving time and energy.

3.2.3.1. Effect of scavengers on the photodegradation process. Various reactive species, such as hydroxyl radicals ($\text{HO}\bullet$), positive holes (h^+), and superoxide anion radicals ($\text{O}_2^{\bullet-}$) can participate in the photocatalytic degradation of organic compounds.

To evaluate the contribution of the main reactive species and to elucidate the photocatalytic mechanism involved in the MG degradation by TP and TP-AC, different scavengers were used. These experiments were carried out under moderate temperature because in these conditions the experiments' execution is simpler and more suited to reality.

The following scavengers have been used in this study.

- 2-propanol. It is a suitable scavenger for hydroxyl radicals that could be produced through the oxidation of both water and hydroxyl groups by the positive holes (h^+) left in the valence band (VB) after the semiconductor excitation upon illumination (Neto et al., 2020).
- Benzoquinone (BQ). It is an appropriate scavenger of superoxide anion radicals ($\text{O}_2^{\bullet-}$) (Schneider et al., 2020). MG molecules could be photosensitized to an excited single state (dye^*) through irradiation, leading to an injection of electrons on the TiO_2 conduction band.

Hence, their reaction with molecular oxygen adsorbed on the catalyst surface would trigger the formation of superoxide anion radicals and/or hydroperoxide radicals (HO_2^\bullet), which would furthermore conduct to the formation of hydroxyl radicals (Cheng et al., 2018; Neto et al., 2020).

- Methanol (MeOH). It is considered a classical holes scavenger (Tan et al., 2003; Schneider et al., 2020).

The results obtained in the tests carried out with scavengers are presented in Fig. 7.

As expected, in the tests carried out with the AC (Fig. 7a), no effect of the scavengers was observed since there was no photodegradation.

In the case of the TP sample (Fig. 7b), the MG photodegradation was strongly inhibited by the presence of benzoquinone, indicating that superoxide anion radicals are highly involved in the photooxidation process, followed by a moderate participation of photogenerated holes, while hydroxyl radicals presented the lowest contribution. That is, the superoxide anion radicals are the major contributors to the photocatalytic degradation of MG and, hence, adding the BQ scavenger caused nearly no MG to be removed by photodegradation (i.e., at 10 min time, 50% MG is removed without scavenger, whereas only 1–2% MG is removed with the BQ scavenger).

The same trend and behavior were observed in the case of using TP-AC, see Fig. 7c, although the relative importance of incorporating scavengers is lower in comparison with TP, as a consequence of adsorption. At 10 min time, adsorption and photodegradation removed

97% of MG in TP-AC. After the addition of the BQ scavenger, 70% of MG was removed, that is, MG was essentially removed by adsorption (although photodegradation also occurs). This highlights that adsorption contributes most to the MG removal from the solution using the TP-AC composite under simulated solar radiation. Bearing in mind that in TP-AC there is 70 wt.% TP (and 30% wt. C), and that within 10 min 50% of MG was removed by photooxidation in TP, in the TP-AC composite around 35% MG should have been removed by photooxidation within 10 min, considering the content of TP, in contrast to 22%, which is an approximate value measured. This tentative data highlights that the presence of AC in TP-AC does not increase the rate of photooxidation concerning what would be oxidized with that amount of TP, but they are of the same order of magnitude or even lower. This would imply that the presence of the highly activated carbon in the composition of the photocatalyst does not enhance the photocatalytic degradation performance of the final material, in which MG removal is dominated by adsorption.

The fact that the presence of the AC in TP-AC does not enhance TP photocatalytic degradation is just opposite from the accepted explanation, claiming the synergy and photooxidation enhancement for TiO_2 -based photocatalysts containing carbons or highly activated carbons, in many cases in gas phase experiments (Bouazza et al., 2008; Lillo-Ródenas et al., 2007), commonly attributed to the pollutant being concentrated (by adsorption) close to the photocatalytic active sites, what would enhance its photooxidation removal (Liu et al., 2007; Paušov et al., 2019). Possibly, the optimum composition of carbon in a hybrid photocatalyst for a given application will also be strongly

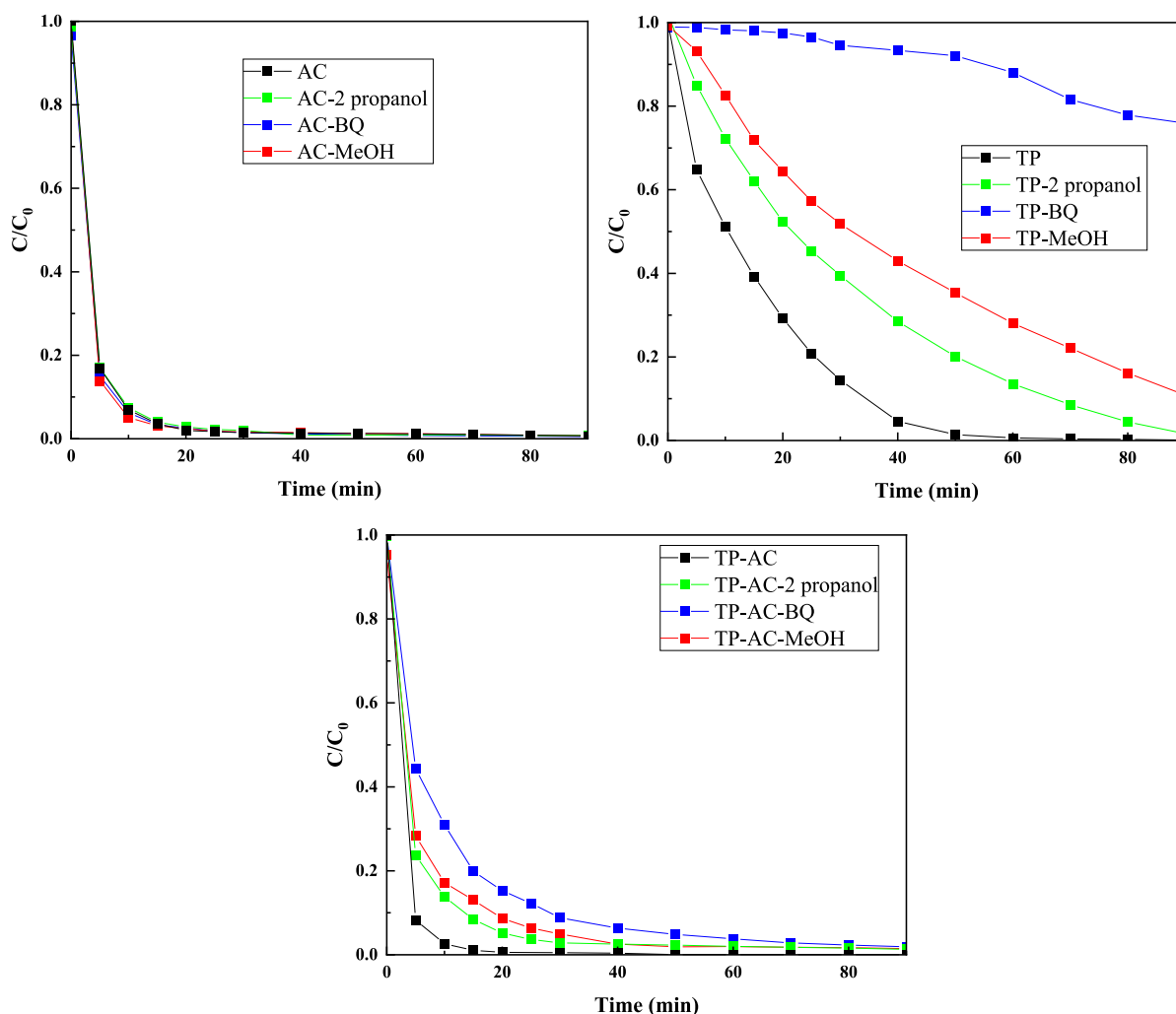


Fig. 7. Photodegradation of MG over a) AC, b) TP, and c) TP-AC in the presence of different scavengers: 2-propanol, BQ, and MeOH.

determined by the reaction media, either liquid or gaseous.

Assuming that the selection of adsorption versus photocatalytic degradation will also be influenced by the type, toxicity, and amount of the degradation products, attention needs to be paid to that as well. The principal photodegradation mechanisms of MG in a variety of photooxidative processes have been reported as the N-demethylation of the MG molecule, and the cleavage of the conjugated structure yields, among others, benzophenone derivatives.

4. Conclusions

The present work has focused on the comparison of malachite green removal under simulated solar light with titanium dioxide P25 (TP) and with a composite containing TP and AC derived from luffa cylindrica (TP-AC), containing 70 wt.% TP and 30 wt.% AC, with the MG removal by adsorption on the luffa cylindrica AC. This study has revealed that in the scenarios and studied conditions, in all cases the total MG removal from solution takes place within the time assayed, 2 h, in some cases with few minutes. The AC presents a very fast and good MG removal by adsorption due to its high surface area (1139 m²/g) and developed porous texture. In the case of TP, there is also total MG removal by photooxidation, although the MG removal process required more than three times that required for the MG adsorption with the AC.

From a kinetic point of view, the TP-AC composite is much more efficient for MG removal from solution than TP, and only slightly more efficient than the AC adsorbent. In such composite, combined adsorption and MG photooxidation take place. In contrast to what could be expected, the incorporation of carbon does not noticeably enhance TP photooxidation. In fact, adsorption dominates the MG removal from solution for the TP-AC composite under simulated solar light.

When using TP for MG photooxidation, the direct photodegradation of MG (avoiding an initial dark period) is more efficient. MG photodegradation by TP occurs via an oxidative process and its oxidation mechanism is dominated by the superoxide anion radicals, although hydroxyl radicals and, especially, holes, also play a role. In such a process, the oxidized malachite green is not totally mineralized, and some intermediate compounds are detected.

For each method, the MG removal results are similar in the two temperature regimes studied, and, in general, the final selection of a removal MG method depends on considerations such as the cost and sustainability (i.e., for the AC preparation and the regeneration step) in the case of adsorption, and the amount and toxicity of the intermediate oxidation compounds and the photocatalysts, as well as the photooxidation energy cost, among others.

CRediT authorship contribution statement

S. Boumad: Writing – review & editing, Writing – original draft, Methodology, Investigation, Formal analysis, Data curation, Conceptualization. **L. Cano-Casanova:** Writing – original draft, Methodology, Investigation, Formal analysis, Data curation. **M.C. Román-Martínez:** Writing – review & editing, Writing – original draft, Validation, Supervision, Resources, Project administration, Methodology, Investigation, Funding acquisition, Formal analysis, Data curation, Conceptualization. **N. Bouchenafa-Saib:** Supervision, Project administration, Methodology, Investigation, Funding acquisition, Data curation, Conceptualization. **M.A. Lillo-Ródenas:** Writing – review & editing, Writing – original draft, Validation, Supervision, Resources, Project administration, Methodology, Investigation, Funding acquisition, Formal analysis, Data curation, Conceptualization.

Declaration of competing interest

The authors declare that they have no known competing financial interests or personal relationships that could have appeared to influence the work reported in this paper.

Data availability

Data will be made available on request.

Acknowledgments

This work was supported by the following research projects: PID2021–123079OB-I00 (project funded by MCIN/AEI/10.13039/501100011033 and by ERDF A way of making Europe (European Union)), CIPROM/2021/070 (Generalitat Valenciana) and VIGROB-136 (University of Alicante). Souad BOUMAD thanks *Mujeres por Africa foundation* for the scholarship offer within the 2019 Learn Africa program and, the Algerian Ministry of Higher Education and Scientific Research for the 2019–2020 scholarship of the P.N.E. program.

Appendix A. Supplementary data

Supplementary data to this article can be found online at <https://doi.org/10.1016/j.envres.2024.118510>.

References

- Ahmad, R., Kumar, R., 2010. Adsorption studies of hazardous malachite green onto treated ginger waste. *J. Environ. Manag.* 91, 1032–1038. <https://doi.org/10.1016/j.jenvman.2009.12.016>.
- Al Bahri, M., Calvo, L., Gilarranz, M.A., Rodríguez, J.J., 2012. Activated carbon from grape seeds upon chemical activation with phosphoric acid: application to the adsorption of diuron from water. *Chem. Eng. J.* 203, 348–356. <https://doi.org/10.1016/j.cej.2012.07.053>.
- Amorós-Pérez, A., Cano-Casanova, L., Castillo-Deltell, A., Lillo-Ródenas, M.Á., Román-Martínez, M. del C., Román-Martínez, M.C., 2018. TiO₂ modification with transition metallic species (Cr, Co, Ni, and Cu) for photocatalytic abatement of acetic acid in liquid phase and propene in gas phase. *Materials* 12, 40. <https://doi.org/10.3390/ma12010040>.
- Andriantsiferana, C., Mohamed, E.F., Delmas, H., 2014. Photocatalytic degradation of an azo-dye on TiO₂/activated carbon composite material. *Environ. Technol.* 35, 355–363. <https://doi.org/10.1080/09593330.2013.828094>.
- Araña, J., Doña-Rodríguez, J.M., Tello Rendón, E., Garriga I Cabo, C., González-Díaz, O., Herrera-Melián, J.A., Pérez-Peña, J., Colón, G., Navio, J.A., 2003. TiO₂ activation by using activated carbon as a support: Part I. Surface characterisation and decantability study. *Appl. Catal. B Environ.* 44, 161–172. [https://doi.org/10.1016/S0926-3373\(03\)00107-3](https://doi.org/10.1016/S0926-3373(03)00107-3).
- Arifin, S.A., Jalaludin, S., Saleh, R., 2015. Photocatalytic decolorization of malachite green in the presence of Fe₃O₄/TiO₂/CuO nanocomposites. In: *Adv. Mater. Res.* Trans Tech Publ 264–269. <https://doi.org/10.4028/www.scientific.net/AMR.1123.264>.
- Bansal, R.C., Goyal, M., 2005. Activated Carbon Adsorption. CRC press.doi: 10.1201/9781420028812.
- Bansal, P., Bhullar, N., Sud, D., 2009. Studies on photodegradation of malachite green using TiO₂/ZnO photocatalyst. *Desalination Water Treat.* 12, 108–113. <https://doi.org/10.5004/dwt.2009.944>.
- Bello, O.S., Ahmad, M.A., Semire, B., 2015. Scavenging malachite green dye from aqueous solutions using pomelo (*Citrus grandis*) peels: kinetic, equilibrium and thermodynamic studies. *Desalination Water Treat.* 56, 521–535. <https://doi.org/10.1080/19443994.2014.940387>.
- Bhatnagar, A., Anastopoulos, I., 2017. Adsorptive removal of bisphenol A (BPA) from aqueous solution: a review. *Chemosphere* 168, 885–902. <https://doi.org/10.1016/j.chemosphere.2016.10.121>.
- Bojinova, A., Kralchevska, R., Poullos, I., Dushkin, C., 2007. Anatase/rutile TiO₂ composites: influence of the mixing ratio on the photocatalytic degradation of Malachite Green and Orange II in slurry. *Mater. Chem. Phys.* 106, 187–192. <https://doi.org/10.1016/j.matchemphys.2007.05.035>.
- Bouazza, N., Lillo-Ródenas, M.A., Linares-Solano, A., 2008. Photocatalytic activity of TiO₂-based materials for the oxidation of propene and benzene at low concentration in presence of humidity. *Appl. Catal. B Environ.* 84, 691–698. <https://doi.org/10.1016/j.apcatb.2008.06.002>.
- Bouchenafa-Saib, N., Grange, P., Verhasselt, P., Addoun, F., Dubois, V., 2005. Effect of oxidant treatment of date pit active carbons used as Pd supports in catalytic hydrogenation of nitrobenzene. *Appl. Catal. Gen.* 286, 167–174. <https://doi.org/10.1016/j.apcata.2005.02.022>.
- Boumad, S., Infantes-Molina, A., Barroso-Martín, I., Moretti, E., Rodríguez-Castellón, E., Román-Martínez, M. del C., Lillo-Ródenas, M.Á., Bouchenafa-Saib, N., 2021. Advantages of the incorporation of luffa-based activated carbon to titania for improving the removal of methylene blue from aqueous solution. *Appl. Sci.* 11, 7607. <https://doi.org/10.3390/app11167607>.
- Cano-Casanova, L., Amorós-Pérez, A., Lillo-Ródenas, M.Á., Román-Martínez, M. del C., 2018. Effect of the preparation method (sol-gel or hydrothermal) and conditions on the TiO₂ properties and activity for propene oxidation. *Materials* 11. <https://doi.org/10.3390/ma11112227>.

- Cano-Casanova, L., Amorós-Pérez, A., Ouzzine, M., Román-Martínez, M.C., Lillo-Ródenas, M.A., 2021. Enhancement of the TiO₂ photoactivity for propene oxidation by carbon incorporation using saccharose in hydrothermal synthesis. *J. Environ. Chem. Eng.* **9**, 104941 <https://doi.org/10.1016/j.jece.2020.104941>.
- Cazorla-Amorós, D., Alcañiz-Monge, J., Linares-Solano, A., 1996. Characterization of activated carbon fibers by CO₂ adsorption. *Langmuir* **12**, 2820–2824. <https://doi.org/10.1021/la960022s>.
- Che Ramlı, Z.A., Asim, N., Isahak, W.N.R.W., Emdadi, Z., Ahmad-Ludin, N., Yarmo, M.A., Sopian, K., 2014. Photocatalytic degradation of methylene blue under UV light irradiation on prepared carbonaceous TiO₂. *Sci. World J.* **13–15**. <https://doi.org/10.1155/2014/415136>, 2014.
- Cheng, X., Zu, L., Jiang, Y., Shi, D., Cai, X., Ni, Y., Lin, S., Qin, Y., 2018. A titanium-based photo-Fenton bifunctional catalyst of mp-MXene/TiO₂-x nanodots for dramatic enhancement of catalytic efficiency in advanced oxidation processes. *Chem. Commun.* **54**, 11622–11625. <https://doi.org/10.1039/c8cc05866k>.
- Cooksey, C., 2016. Quirks of dye nomenclature. 6. Malachite green. *Biotech. Histochem.* **91**, 438–444. <https://doi.org/10.1080/10520295.2016.1209787>.
- Cruz, G.J.F., Gómez, M.M., Solis, J.L., Rimaycuna, J., Solis, R.L., Cruz, J.F., Rathnayake, B., Keiski, R.L., 2018. Composites of ZnO nanoparticles and biomass based activated carbon: adsorption, photocatalytic and antibacterial capacities. *Water Sci. Technol.* **492–508**. <https://doi.org/10.2166/wst.2018.176>, 2017.
- Das, A.K., Saha, S., Pal, A., Maji, S.K., 2009. Surfactant-modified alumina: an efficient adsorbent for malachite green removal from water environment. *J. Environ. Sci. Heal. - Part A Toxic/Hazardous Subst. Environ. Eng.* **44**, 896–905. <https://doi.org/10.1080/10934520902958708>.
- Devi, L.G., Kavitha, R., 2014. Enhanced photocatalytic activity of sulfur doped TiO₂ for the decomposition of phenol: a new insight into the bulk and surface modification. *Mater. Chem. Phys.* **143**, 1300–1308. <https://doi.org/10.1016/j.matchemphys.2013.11.038>.
- El-Zahhar, A.A., Awwad, N.S., 2016. Removal of malachite green dye from aqueous solutions using organically modified hydroxyapatite. *J. Environ. Chem. Eng.* **4**, 633–638. <https://doi.org/10.1016/j.jece.2015.12.014>.
- Farooqi, Z.H., Sultana, H., Begum, R., Usman, M., Ajmal, M., Nisar, J., Irfan, A., Azam, M., 2020. Catalytic degradation of malachite green using a crosslinked colloidal polymeric system loaded with silver nanoparticles. *Int. J. Environ. Anal. Chem.* <https://doi.org/10.1080/03067319.2020.1779247>.
- Fischer, A.R., Werner, P., Goss, K.U., 2011. Photodegradation of malachite green and malachite green carbinol under irradiation with different wavelength ranges. *Chemosphere* **82**, 210–214. <https://doi.org/10.1016/j.chemosphere.2010.10.019>.
- Fu, P., Luan, Y., Dai, X., 2004. Preparation of TiO₂ photocatalyst anchored on activated carbon fibers and its photodegradation of methylene blue. *China Particuol.* **2**, 76–80. [https://doi.org/10.1016/S1672-2515\(07\)60027-X](https://doi.org/10.1016/S1672-2515(07)60027-X).
- Gao, X., Wang, Z., Zhai, X., Fu, F., Li, W., 2015. The synthesis of lanthanide doped BiVO₄ and its enhanced photocatalytic activity. *J. Mol. Liq.* **211**, 25–30. <https://doi.org/10.1016/j.molliq.2015.06.058>.
- Guimarães, J.R., Guedes Maniero, M., Nogueira de Araújo, R., 2012. A comparative study on the degradation of RB-19 dye in an aqueous medium by advanced oxidation processes. *J. Environ. Manag.* **110**, 33–39. <https://doi.org/10.1016/j.jenvman.2012.05.020>.
- Hernández, V., 2012. Lignocellulosic Precursors Used in the Synthesis of Activated Carbon - Characterization Techniques and Applications in the Wastewater Treatment. InTech. <https://doi.org/10.5772/3346>.
- Ju, Y., Yang, S., Ding, Y., Sun, C., Zhang, A., Wang, L., 2008. Microwave-assisted rapid photocatalytic degradation of malachite green in TiO₂ suspensions: mechanism and pathways. *J. Phys. Chem. A* **112**, 11172–11177. <https://doi.org/10.1021/jp804439z>.
- Kisch, H., 2015. *Semiconductor Photocatalysis Principles and Applications*. Wiley-VCH Verlag GmbH & Co. <https://doi.org/10.1002/9783527673315>.
- Kosmulski, M., 2021. The pH dependent surface charging and points of zero charge. IX. Update. *Adv. Colloid Interface Sci.* **296**, 102519 <https://doi.org/10.1016/j.cis.2021.102519>.
- Kummert, R., Stumm, W., 1980. The surface complexation of organic acids on hydrous γ-Al₂O₃. *J. Colloid Interface Sci.* **75**, 373–385. [https://doi.org/10.1016/0021-9797\(80\)90462-2](https://doi.org/10.1016/0021-9797(80)90462-2).
- László, K., 2005. Adsorption from aqueous phenol and aniline solutions on activated carbons with different surface chemistry. *Colloids Surfaces A Physicochem. Eng. Asp.* **265**, 32–39. <https://doi.org/10.1016/j.colsurfa.2004.11.051>.
- Lavand, A.B., Bhatu, M.N., Malghe, Y.S., 2019. Visible light photocatalytic degradation of malachite green using modified titania. *J. Mater. Res. Technol.* **8**, 299–308. <https://doi.org/10.1016/j.jmrt.2017.05.019>.
- Lillo-Ródenas, M.A., Bouazza, N., Berenguer-Murcia, A., Linares-Salinas, J.J., Soto, P., Linares-Solano, A., 2007. Photocatalytic oxidation of propene at low concentration. *Appl. Catal. B Environ.* **71**, 298–309. <https://doi.org/10.1016/j.apcatb.2006.10.004>.
- Lin, Z., Wang, D., Zhang, H., Li, L., Huang, Z., Shen, J., Lin, Y., 2016. Extraction and determination of malachite green from aquatic products based on molecularly imprinted polymers. *Separ. Sci. Technol.* **51**, 1684–1689. <https://doi.org/10.1080/01496395.2016.1175478>.
- Liu, S.X., Chen, X.Y., Chen, X., 2007. A TiO₂/AC composite photocatalyst with high activity and easy separation prepared by a hydrothermal method. *J. Hazard Mater.* **143**, 257–263. <https://doi.org/10.1016/j.jhazmat.2006.09.026>.
- Lucas, M.S., Tavares, P.B., Peres, J.A., Faria, J.L., Rocha, M., Pereira, C., Freire, C., 2013. Photocatalytic degradation of Reactive Black 5 with TiO₂-coated magnetic nanoparticles. *Catal. Today* **209**, 116–121. <https://doi.org/10.1016/j.cattod.2012.10.024>.
- Matos, J., Laine, J., Herrmann, J.M., 2001. Effect of the type of activated carbons on the photocatalytic degradation of aqueous organic pollutants by UV-irradiated titania. *J. Catal.* **200**, 10–20. <https://doi.org/10.1006/jcat.2001.3191>.
- Morawski, A., Janus, M., Tryba, B., Toyoda, M., Tsumura, T., Inagaki, M., 2009. Carbon modified TiO₂ photocatalysts for water purification. *Pol. J. Chem. Technol.* **11**, 46–50. <https://doi.org/10.2478/v10026-009-0023-0>.
- Neto, J.S.G., Satyro, S., Saggiaro, E.M., Dezotti, M., 2020. Investigation of mechanism and kinetics in the TiO₂ photocatalytic degradation of Indigo Carmine dye using radical scavengers. *Int. J. Environ. Sci. Technol.* **18**, 163–172. <https://doi.org/10.1007/s13762-020-02842-6>.
- Nitniphthut, P., Thabuoit, M., Seithanabutara, V., 2017. Fabrication of composite supercapacitor containing para wood-derived activated carbon and TiO₂. *Energy Proc.* **138**, 116–121. <https://doi.org/10.1016/j.egypro.2017.10.074>.
- Ohtani, B., Prieto-Mahoney, O.O., Li, D., Abe, R., 2010. What is Degussa (Evonik) P25? Crystalline composition analysis, reconstruction from isolated pure particles and photocatalytic activity test. *J. Photochem. Photobiol. Chem.* **216**, 179–182. <https://doi.org/10.1016/j.jphotochem.2010.07.024>.
- Pašová, Š., Riva, M., Baudys, M., Krýsa, J., Barbieriková, Z., Brezová, V., 2019. Composite materials based on active carbon/TiO₂ for photocatalytic water purification. *Catal. Today* **328**, 178–182. <https://doi.org/10.1016/j.cattod.2019.01.010>.
- Pérez-Estrada, L.A., Agüera, A., Hernando, M.D., Malato, S., Fernández-Alba, A.R., 2008. Photodegradation of malachite green under natural sunlight irradiation: kinetic and toxicity of the transformation products. *Chemosphere* **70**, 2068–2075. <https://doi.org/10.1016/j.chemosphere.2007.09.008>.
- Reddy, L.S., Ko, Y.H., Yu, J.S., 2015. Hydrothermal synthesis and photocatalytic property of β-Ga₂O₃ nanorods. *Nanoscale Res. Lett.* **10** <https://doi.org/10.1186/s11671-015-1070-5>.
- Regalbuto, J.R., 2006. *Surface and Nanomolecular Catalysis*. CRC Press. <https://doi.org/10.1201/9781420015751>.
- Rodriguez-Reinoso, F., Linares-Solano, A., 1988. In: Thrower, PA (Ed.). In: *Chemistry and Physics of Carbon*. 21. Marcel Dekker, New York, pp. 1–146. [https://doi.org/10.1016/0008-6223\(78\)90047-7](https://doi.org/10.1016/0008-6223(78)90047-7).
- Romero-Anaya, A.J., Lillo-Ródenas, M.A., Salinas-Martínez De Lecea, C., Linares-Solano, A., 2012. Hydrothermal and conventional H₃PO₄ activation of two natural bio-fibers. *Carbon N. Y.* **50**, 3158–3169. <https://doi.org/10.1016/j.carbon.2011.10.031>.
- Sayilkan, F., Asiltürk, M., Tatar, P., Kiraz, N., Arpaç, E., Sayilkan, H., 2007. Photocatalytic performance of Sn-doped TiO₂ nanostructured mono and double layer thin films for Malachite Green dye degradation under UV and vis-lights. *J. Hazard Mater.* **144**, 140–146. <https://doi.org/10.1016/j.jhazmat.2006.10.011>.
- Schneider, J.T., Firak, D.S., Ribeiro, R.R., Peralta-Zamora, P., 2020. Use of scavenger agents in heterogeneous photocatalysis: truths, half-truths, and misinterpretations. *Phys. Chem. Chem. Phys.* **22**, 15723–15733. <https://doi.org/10.1039/d0cp02411b>.
- Shahcheragh, S.K., Bagheri Moghagheghi, M.M., Shirpay, A., 2023. Effect of physical and chemical activation methods on the structure, optical absorbance, band gap and urbach energy of porous activated carbon. *SN Appl. Sci.* **5** <https://doi.org/10.1007/s42452-023-05559-6>.
- Sing, K.S.W., Rouquerol, F., Rouquerol, J., 2014. Classical interpretation of physisorption isotherms at the gas–solid interface, adsorpt. By powders porous solids princ. In: *Methodol. Appl.*, second ed., pp. 159–189. <https://doi.org/10.1016/B978-0-08-097035-6.00005-X>.
- Slimen, H., Houas, A., Nogier, J.P., 2011. Elaboration of stable anatase TiO₂ through activated carbon addition with high photocatalytic activity under visible light. *J. Photochem. Photobiol. Chem.* **221**, 13–21. <https://doi.org/10.1016/j.jphotochem.2011.04.013>.
- Song, J., Han, G., Wang, Y., Jiang, X., Zhao, D., Li, M., Yang, Z., Ma, Q., Parales, R.E., Ruan, Z., 2020. Pathway and kinetics of malachite green biodegradation by *Pseudomonas veronii*. *Sci. Rep.* **10**, 4502. <https://doi.org/10.1038/s41598-020-61442-z>.
- Srivastava, S., Sinha, R., Roy, D., 2004. Toxicological effects of malachite green. *Aquat. Toxicol.* **66**, 319–329. <https://doi.org/10.1016/j.aquatox.2003.09.008>.
- Tan, T., Beydoun, D., Amal, R., 2003. Effects of organic hole scavengers on the photocatalytic reduction of selenium anions. *J. Photochem. Photobiol. Chem.* **159**, 273–280. [https://doi.org/10.1016/S1010-6030\(03\)00171-0](https://doi.org/10.1016/S1010-6030(03)00171-0).
- Thommes, M., Kaneko, K., Neimark, A.V., Olivier, J.P., Rodriguez-Reinoso, F., Rouquerol, J., Sing, K.S.W., 2015. Physisorption of gases, with special reference to the evaluation of surface area and pore size distribution (IUPAC Technical Report). *Pure Appl. Chem.* **87**, 1051–1069. <https://doi.org/10.1515/pac-2014-1117>.
- Wang, X., Zhou, J., Zhao, S., Chen, X., Yu, Y., 2018. Synergistic effect of adsorption and visible-light photocatalysis for organic pollutant removal over BiVO₄/carbon sphere nanocomposites. *Appl. Surf. Sci.* **453**, 394–404. <https://doi.org/10.1016/j.apsusc.2018.05.073>.
- Xu, T., Liu, X., 2008. Peanut shell activated carbon: characterization, surface modification and adsorption of Pb²⁺ from aqueous solution. *Chin. J. Chem. Eng.* **16**, 401–406. [https://doi.org/10.1016/S1004-9541\(08\)60096-8](https://doi.org/10.1016/S1004-9541(08)60096-8).
- Yong, L., Zhanqi, G., Yuefei, J., Xiaobin, H., Cheng, S., Shaogui, Y., Lianhong, W., Qingeng, W., Die, F., 2015. Photodegradation of malachite green under simulated and natural irradiation: kinetics, products, and pathways. *J. Hazard Mater.* **285**, 127–136. <https://doi.org/10.1016/j.jhazmat.2014.11.041>.
- Zhang, W., Huang, Y., Liu, P., Zhao, Y., Wu, H., Guan, M., Zhang, H., 2014. TiO₂ supported on bamboo charcoal for H₂O₂-assisted pollutant degradation under solar light. *Mater. Sci. Semicond. Process.* **17**, 124–128. <https://doi.org/10.1016/j.mssp.2013.08.014>.